Research Square

Preprints are preliminary reports that have not undergone peer review.
They should not be considered conclusive, used to inform clinical practice,
or referenced by the media as validated information.

Methods for characterization of atomic-scale field emission point-electron-source

Shaozhi Deng

stsdsz@mail.sysu.edu.cn

State Key Lab of Optoelectronic Materials and Technologies, Guangdong Province Key Lab of Display Material and Technology, School of Electronics and Information Technology, Sun Yat-sen University

https://orcid.org/0000-0003-1830-2026

Shuai TANG

https://orcid.org/0000-0003-0086-9104

Mingkai Gou

State Key Lab of Optoelectronic Materials and Technologies, Guangdong Province Key Lab of Display Material and Technology, School of Electronics and Information Technology, Sun Yat-sen University

Yingzhou Hu

State Key Lab of Optoelectronic Materials and Technologies, Guangdong Province Key Lab of Display Material and Technology, School of Electronics and Information Technology, Sun Yat-sen University

Jie Tang

Faculty of Materials and Manufacturing, Beijing University of Technology, Beijing 100124, China

Yan Shen

State Key Lab of Optoelectronic Materials and Technologies, Guangdong Province Key Lab of Display Material and Technology, School of Electronics and Information Technology, Sun Yat-sen University

Yu Zhang

State Key Lab of Optoelectronic Materials and Technologies, Guangdong Province Key Lab of Display Material and Technology, School of Electronics and Information Technology, Sun Yat-sen University

Lu-chang Qin

Faculty of Materials and Manufacturing, Beijing University of Technology, Beijing 100124, China

Ningsheng Xu

Guangdong Province Key Laboratory of Display Material and Technology, School of Electronics and Information Technology, Sun Yat-sen University

Richard Forbes

School of Mathematics and Physics, University of Surrey, Guildford, Surrey GU2 7XH, United Kingdom

---

Article

Keywords: Field emission, Fowler-Nordheim FE theory, Murphy-Good FE theory, field ion microscopy, field electron microscopy, emission area, atomic-scale

Posted Date: March 4th, 2026

DOI: https://doi.org/10.21203/rs.3.rs-8883179/v1

License: This work is licensed under a Creative Commons Attribution 4.0 International License.
Read Full License

Additional Declarations: There is **NO** Competing Interest.

Methods for characterization of atomic-scale field emission point-electron-source

Shuai Tang[1], Mingkai Gou[1], Yingzhou Hu[1], Jie Tang[2], Yan Shen[1], Yu Zhang[1], Lu-chang Qin[2], Ningsheng Xu[1], Richard G. Forbes[3], Shaozhi Deng[1]*

[1]State Key Laboratory of Optoelectronic Materials and Technologies, Guangdong Province Key Laboratory of Display Material and Technology, School of Electronics and Information Technology, Sun Yat-sen University, Guangzhou 510275, China

[2]Faculty of Materials and Manufacturing, Beijing University of Technology, Beijing 100124, China

[3]School of Mathematics and Physics, University of Surrey, Guildford, Surrey GU2 7XH, United Kingdom

Corresponding Author E-mail: stsdsz@mail.sysu.edu.cn

Abstract

Field emission (FE) electron sources are made close to atomic-scale to reach the highest spatial resolution as well as stable emission for electron microscopy, electron beam inspection and lithography. At present, no single agreed method exists of using FE current-voltage data to extract the apparent emission area, which is needed for predicting some beam properties. The 1956 theory of Murphy and Good (MG) is better physics than the 1920s theory of Fowler and Nordheim (FN) and colleagues, but many researchers use simplified FN theory to analyse experimental data. The present paper reports an experimental method of finding apparent emission area, based on using field ion and field electron microscopes (FIM-FEM). The discrepancy of emission area between the FIM-FEM method and MG-based analysis is a factor of 7.4, while that with simplified FN-based analysis is about 25, confirming MG theory is better for FE data analysis. The result allows deduction of key indicators, including source energy spread, reduced brightness and emission efficiency. A downloadable program is made available to help analysis. Our work provide a new experimental method of characterizing FE electron sources, especially the atomic-scale cold cathode, for which existing plot-based data-analysis methods are not suitable.

Keywords: Field emission, Fowler-Nordheim FE theory, Murphy-Good FE theory, field ion microscopy, field electron microscopy, emission area, atomic-scale.

1. Background

Electron microscopy has a wide range of applications in integrated circuits, materials science, structural biology, and ultrafast science. With the miniaturization of chip structures [1, 2] and the development of cryo-electron microscopy [3, 4], ultra-fast electron microscopy [5], in situ liquid electron microscopy [6] and other new technologies, electron microscopes need extremely high spatial resolution at the picometer level [7, 8] and temporal resolution at the attosecond level [9]. The spatial resolution of an electron microscope is determined by the virtual source characteristics, the spherical aberration of the electromagnetic lens, chromatic aberration of the electron beam, and diffraction of the electron beam [10–12]. Since spherical aberration issues have been resolved [13, 14] and diffraction is determined by the accelerating voltage, the characteristics of the electron source (including size and energy spread) become the key factors limiting the spatial resolution of the electron microscope [15]. Emission induced by a highly negative electrostatic (ES) field is called here "field electron emission" (FE). Compared with other cathode types, FE sources offer the highest brightness and the narrowest total-energy spread. These things bring benefits for high-resolution imaging and spectroscopy. Since the pioneering FE theory reported in 1928 [16], various materials including metals [17, 18], metal oxides [19–21], carbon-based nanostructures [22–24], metal carbides [25–27] and rare-earth hexaborides [28–30] have been investigated and used as cold cathodes.

The lanthanum hexaboride (LaB_6) cold cathode, with apex radius around 10 nm, exhibits outstanding performance. It has better signal-to-noise characteristics than a tungsten cold cathode, and good resolution inside a SEM [31]. Our recently developed [28] very-fine-tip LaB_6-nanocone cold cathode, fabricated by a FIB-based method, performs better than commercial tungsten sources when operated in a spherical-aberration-corrected TEM [28, 32]. This LaB_6 FE source exhibits equivalent high spatial resolution, one third lower energy spread, and more than tenfold enhanced stability of tungsten FE source.

Much of this excellent source behaviour can be attributed to its small apex radius of 10 nm. This results in a smaller virtual source size as well as more stable emission characteristics. Particularly with the growing use of small-apex-radius emitters, it is very desirable to establish theoretical and experimental methodologies for more accurate analysis of the performance of FE sources in general.

FE theory involves quantum tunnelling. The 1928 Fowler-Nordheim (FN) paper [16] evaluated tunnelling probabilities by using an exactly triangular (ET) tunnelling barrier. This approach ignored image-potential-energy (PE) effects. This incorrect approach is also used when deriving the elementary FE equation, which often appears in technological FE papers and is written here as

$$I_{\mathrm{m}}^{\mathrm{EL}} = \frac{A_{\mathrm{f}}^{\mathrm{ET}} a\beta^2 V_{\mathrm{m}}^2}{\phi} \exp\left(\frac{-b\phi^{\frac{3}{2}}}{\beta V_{\mathrm{m}}}\right), \tag{1}$$

where a [$\approx 1.541\times10^{-6}$ A eV V^{-2}] and $b \approx 6.831\times10^{9}$ eV$^{-3/2}$ V m^{-1}] are the FN universal constants [see electronic supplementary material (ESM)], and $A_{\mathrm{f}}^{\mathrm{ET}}$ is the formal emission area derived by assuming an ET barrier. The parameter β that links the magnitude F_{a} of the electrostatic field at the emitter apex to V_{m} is defined via

$$F_{\mathrm{a}} = \beta V_{\mathrm{m}}. \tag{2}$$

β is called here the (voltage-to-apex-field) *conversion factor (CF)*. For so-called *electronically ideal* systems β can be treated as constant (see ESM for details).

Later in 1928 [33], Nordheim realized that including image PE effects, to give what is now called the Schottky-Nordheim (SN) tunnelling barrier (see ESM), leads to a correction factor in the exponent of eq. (1). Unfortunately, he made a mathematical mistake [34]. In the 1950s [35], Burgess, Kroemer and Houston (BKH) suggested that the correction factor should be a particular value of a mathematical function denoted here by $\mathrm{v}_{\mathrm{BKH}}(y)$, where y is the *Nordheim parameter* (see ESM). Murphy and Good [36] then developed a replacement for the 1928 FN FE equation. This replacement is called here the 1956 Murphy-Good (MG) FE equation.

A modern development is the so-called "Extended" (or "Experiment-oriented") MG (EMG) FE equation:

$$I_{\mathrm{m}}^{\mathrm{EMG}} = \frac{A_{\mathrm{f}}^{\mathrm{SN}} a\beta^2 V_{\mathrm{m}}^2}{\phi} \exp\left(\frac{-\mathrm{v}_{\mathrm{FD}}(f)\cdot b\phi^{\frac{3}{2}}}{\beta V_{\mathrm{m}}}\right). \tag{3}$$

Here $I_{\mathrm{m}}^{\mathrm{EMG}}$ is the measured current (as described by EMG theory) and $A_{\mathrm{f}}^{\mathrm{SN}}$ is the formal emission area derived by assuming a SN barrier. The parameter f is the so-called *scaled field* (see ESM), and $\mathrm{v}_{\mathrm{FD}}(f)$ is a particular value of a special mathematical function introduced by Forbes and Deane (see [37] and ESM). Because it is close to unity, the factor t^{-2} in the 1956 MG FE zero-temperature equation has been absorbed into $A_{\mathrm{f}}^{\mathrm{SN}}$.

Both eq. (1) and eq. (3) lead to area extraction procedures, at present usually based on FN plots. However, the formal area extracted by assuming a SN barrier is much less (by a factor of 100 or more) than the formal area extracted by assuming an ET barrier. Thus, it is of practical interest which barrier is the better approximation to reality, since this affects the numerical values deduced from current-voltage experiments for current densities, brightness and other key indicators of a field emitting electron source. It is theoretically certain that assuming a SN barrier is better physics than assuming an ET barrier, and that MG-type FE theory is better physics than 1920s FE theory [34]. However, for scientific completeness it would be useful to also have experimental proofs of this.

A useful approach was developed in 1973 by Ehrlich and Plummer [38], who attempted direct measurement of the local emission current density (LECD) from a tungsten (110) plane. They found, as theoretically expected, that the experimental results were significantly closer to MG FE theory than to elementary FE theory. Their conclusion seems qualitatively valid, but interpretation of their results is not without its difficulties and the emission area cannot be accurately obtained from their approach.

This paper aims to provide a new experimental method for measuring the source area of a single needle-like electron source. This new method is expected to work both for relatively blunt emitters and for sharp emitters for which the planar emission approximation (used in deriving emission current formulas—see ESM) seriously breaks down. Thus, our method will work for the upcoming atomic-scale cold cathode. Further, for "not too sharp" emitters, the new method provides further experimental evidence that MG FE theory is more accurate than elementary FE theory.

2. Experimental and theoretical methods

Our new approach is based on the techniques of field ion microscopy (FIM) and field electron microscopy (FEM) and related theory, and involves investigations to determine the linear and area magnifications that apply to these techniques, in particular to our specific experimental system. Our thinking is that, if the area magnification can be successfully determined, then the total area of a FEM screen image can be converted back to an electron-source area on the emitter, and that this constitutes an alternative method of extracting emission area.

It is simple and convenient to calculate linear and area magnifications when using a sharply pointed electron source. A sharp source prepared from a HfC nanowire has been chosen for these FIM-FEM measurements.

2.1 Simulation methods for obtaining the particle trajectories in FIM and FEM

An initial requirement is using finite-element calculations to confirm that (a) electrons in FEM and (b) hydrogen (H_2^+) ions in FIM follow essentially the same trajectories if both start with zero kinetic energy, and hence that the two microscopies have the same transverse and area magnifications.

Our simulations used the following geometry, based on our experimental system. The emitter is modelled as a narrow-angle cone with a rounded apex of radius from 5 nm to 25 nm. The spacing between the emitter and an extractor ring is 2 mm; the ring diameter is 10 mm. The extractor voltage is set to 0 V. A microchannel-plate detector is at a distance 50 mm from the emitter apex, with its beam-facing surface also at 0 V. The electron/ion source radius (R_{emission}) at the emitter tip

is set from 0.5 nm to 2 nm. Several particle-monitoring surfaces along the system axis record particle behaviour at different positions along their trajectories. The distribution area, velocity, angle relative to the axis and other physical quantities were thus monitored at different distances from emitter apex. Simulations used the CST Studio Suite. In the FIM simulation, using H_2^+ ions, the emitter voltage is set as +2000 V; the electrostatic (ES) field at the emitter apex is found as about 37 V/nm. In the FEM simulation, using electrons, the emitter voltage is set as –150 V; the apex ES field is found as –2.76 V/nm.

2.2 FIM and FEM experimental methods

The common emitter used in both FIM and FEM was prepared, by electropolishing and then in-situ field evaporation in FIM mode, from a [100]-oriented single-crystal HfC-nanowire emitter with a square cross-section of side-length 80 nm. The resulting apex radius was approximately 25 nm. The FIM experiments were carried out at room temperature with a background pressure of 1.0×10^{-7} Pa. This situation is not ideal, but is what our current experimental system allows. The operating-gas (H_2) pressure was about 6.5×10^{-4} Pa. The emitter voltage was between +2000 V and +5000 V. Operating-gas molecules are field-ionized close to the emitter surface. Resulting ions are guided by the field to hit the microchannel-plate: this generates a FIM image on a phosphor screen, as shown in Fig. 1(a).

The FEM experiments were conducted in the same apparatus, using a high vacuum of 1.0×10^{-7} Pa and with emitter voltages between –400 V and –1000 V. Field emitted electrons produce at the microscope screen an image of the electron source of area A^S on the emitter tip, as shown in Fig. 1(b). Comparing the results of the FEM and FIM experiments, taking into account the known crystallography of the emitter apex, enables an estimate of A^S, as described below.

2.3 The FN-plot method

Discussion here uses the SI unit "volt" (V) for measured voltage V_m and the SI unit "ampere" for measured current I_m. Related data plots are made in the " *FN coordinates*" $\ln\{I_m/V_m^2\}$ vs V_m^{-1}.

MG theory predicts FN plots to be slightly curved [35, 39], more so at the left-hand (high-voltage) side. This creates errors if plot analysis uses ET-barrier theory, but mathematical complications when SN-barrier theory is used. The theory needed for the SN-barrier case is discussed elsewhere (Appendix to [40]), and set out in the ESM. A summary follows.

Let the straight line fitted to an experimental FN plot have the form

$$L^{expt}(V_m^{-1}) \equiv \ln\{I_m/V_m^2\} = \ln\{R^{expt}\} + S^{expt}/V_m, \quad (4)$$

where R^{expt} and S^{expt} are parameters expressed in A/V^2 and Np V, respectively, with S^{expt} negative.

A validity check, such as the orthodoxy test [41], should be used to investigate whether the

related FE system is electronically ideal. If this is passed (or if the results are indecisive but are close to the pass range), then values of R^{expt}, S^{expt}, and the combination $[R^{expt} \cdot (S^{expt})^2]$ are recorded, as in Table 1 below.

To implement data analysis, this paper uses the parameter "scaled field" (f above) and the related modern version of the tangent method (see ESM).

Strictly, the fitted line $L^{expt}(V_m^{-1})$ is a chord to the data points [42]. The tangent method models this chord by a tangent to the chosen theoretical equation when this theoretical equation is formulated and plotted in FN coordinates. This approach is a good approximation.

The theoretical tangent must be taken at the value of V_m^{-1} at which this tangent is parallel to the experimental chord. This V_m-value is called the *fitting value* and denoted by V_t. Corresponding to V_t there are fitting values F_t of apex "field" and f_t of the related scaled field. Best estimates of V_t, F_t and f_t are initially undecided.

FN-plot analysis involves three correction functions defined in the ESM: the function $v_{FD}(f)$ discussed earlier; the slope correction function $s(f)$; and the intercept correction function $r(\phi, f)$. For simplicity, the fitting values of $s(f)$ and $r(\phi, f)$ are denoted by s_t and r_t, respectively.

Extracted values of the conversion factor β and of the formal emission area A_f^{SN} that appear in eq. (3) are given by (see ESM):

$$\beta^{extr} = -s_t\, b\phi^{3/2} / S^{expt}, \tag{5}$$

$$\{A_f^{SN}\}^{extr} = \Lambda_{FN}^{SN} \cdot [R^{expt}\,(S^{expt})^2]\,, \tag{6}$$

where the *area extraction parameter*, Λ_{FN}^{SN}, for a FN plot, assuming a SN barrier, is

$$\Lambda_{FN}^{SN} = 1/[(ab^2\phi^2) \cdot (r_t s_t^2)]. \tag{7}$$

Formulae for FN-plot analysis using the ET barrier are obtained by setting r_t=1 and s_t=1 (see ESM).

When SN-barrier theory is used, a procedure is needed for determining "best estimates" for s_t and r_t. The procedure used in this paper is described in Section 4.2 and the ESM.

3. Results and discussion

3.1 Simulation results for magnification ratio between FIM and FEM

Figure 1(a) shows how the radius of the emitted electron or ion beam (i.e., the radius of its envelope) varies with distance along the system axis, measured from the emitter surface. Red dots show H_2^+ data and green dots electron data: the two lines of dots overlap perfectly. The blue circles show the ratio of FEM-results/FIM-results: this ratio has a constant value of 1.00. Thus, these simulations show that electrons and H_2^+ ions emitted with zero kinetic energy from a given point

on the emitter surface follow the same trajectory. Historically, this has been a widely accepted result, but it is difficult to find any formal theoretical proof.

In a FIM or FEM, a distance ρ_{scr} on the microscope screen corresponds to a distance ρ_{em} on the emitter surface. The microscope's *linear magnification* m_{lin} is defined as ρ_{scr}/ρ_{em}. The simplest assumption, made here, is that m_{lin} has the same constant value for all parts of the image and all directions in the image. The microscope's area magnification M is then given by $M = (m_{lin})^2$.

For the microscope geometry and assumed emitter shape described above, we investigated how the area magnification M depends on the apex radius-of-curvature and on the radius $R_{emission}$ of the source area. Results are shown in Fig. 1(b). As expected, the area magnification is mainly affected by the apex radius-of-curvature. The source radius does not significantly affect the area magnification. For our experimental emitter of apex radius about 25 nm, the linear magnification predicted by these simulations is about 1.4×10^6.

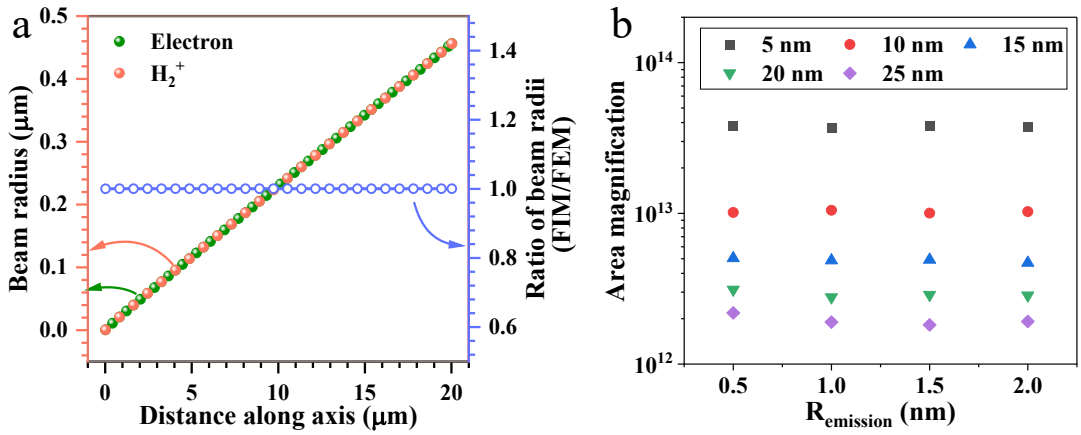


Fig. 1. Data relating to the charged-particle optics of field electron and field ion microscopes. (a) To show how ion (H_2^+) and electron beam radii vary with distance along the system axis (results derived by finite-element simulations). (b) To show how the area magnification varies with the radius $R_{emission}$ of the emission area, for different values of the apex-radius-of-curvature (top figures).

3.2 Deriving electron source area by using FIM&FEM charged-particle optics

Since the FEM area magnification M_{FEM} has been proven the same as the FIM area magnification M_{FIM}, the electron source area A^S on the emitter can be found by using the formula $A^S = A^{FEM}/M_{FIM}$, where A^{FEM} is the area of the FEM-mode image spot on the microscope screen. Fig. 2(b) shows a typical FEM image for the HfC nanowire with an oxycarbide surface. M_{FIM} and A^{FEM} are found as follows.

After preparation for microscopy, the nanowire has a relatively sharp tip, with apex radius about 25 nm. HfC has a "rock-salt" crystal structure, which is a form of face-centred-cubic (fcc)

structure, and has a lattice constant $c_{\mathrm{HfC}} = 0.456$ nm. The central lattice plane in the FIM image (Fig. 2(a)) is the 001 plane. In this plane the nearest-neighbour separation is $c_{\mathrm{HfC}}/\sqrt{2} = 0.322$ nm [43].

Although image quality is limited, we consider that we can identify two adjacent atoms in the net plane. In Fig. 2(a) the centres of the corresponding image spots are joined by a red line. On the photographic record the length of this line is 1.7 mm. The actual separation of spot centres on the microscope screen is determined as follows.

The channel plate has a small hole of known diameter 2.0 mm. We assume that its circumference is, in effect, imaged directly onto the microscope screen as a 2 mm diameter circle. It thus appears in our photographic image record, where its diameter is measured as 4.5 mm. Assuming magnification can be treated as uniform across the image, it follows that distance ρ_{rec}

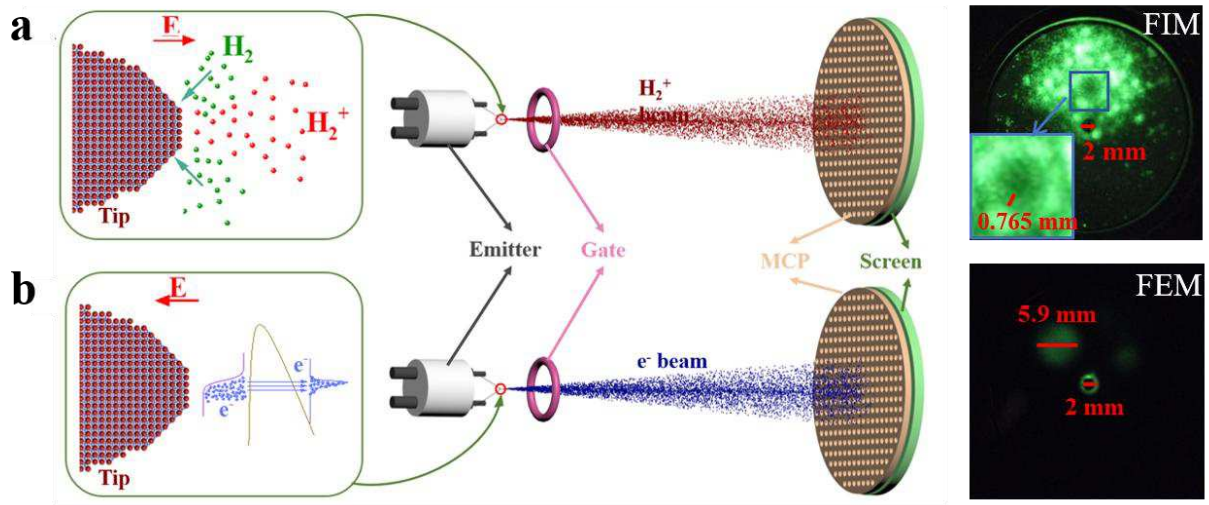


Fig. 2. (a) Schematic diagram of FIM operation, and FIM image of HfC emitter. (b) Schematic diagram of FEM operation, and FEM image of same HfC emitter.

on the image record is converted to distance ρ_{FIM} on the microscope screen by $\rho_{\mathrm{FIM}} = \rho_{\mathrm{rec}}/2.25$. This yields the actual separation of the adjacent image-spot centers on the microscope screen as 0.76 mm.

In the (001) net plane, the nearest-neighbour distance (both between Hf atoms and between C atoms) is $c_{\mathrm{HfC}}/\sqrt{2} = 0.322$ nm. As shown in Table 1, this yields, for the geometry of our microscope and HfC specimen, a linear magnification of about 2.4×10^6. For comparison, the simulation result was about 1.4×10^6. Given our limited knowledge of the experimental emitter shape, this degree of agreement is considered very satisfactory.

The field emitted electrons produce at the microscope screen an image of the electron source area on the emitter tip, as shown in Fig. 2(b). An initial estimate of the physical radius of the screen

image can be found, as above, by making use of the known dimensions of the channel-plate hole, and is recorded in Table 1.

However, we also need to take into account the possible influence of beam effects that would tend to expand the image laterally. These include (e.g., [44], p. 1005) expansion due to mean space-charge effects and expansion associated with the Boersch spatial effect which results from stochastic coulomb interactions. Due to current-density differences, these effects could be significant for electrons but not for H_2^+ ions. If a broadening effect occurs, it would be necessary to divide the initial spot-estimate deduced above by a correction factor related to this effect.

Table 1: Data relating to FIM and FEM experiments. (For precision in calculations, intermediate values are shown to 3 significant figures. Accuracy of final result is not better than 10%.)

Line	Parameter	Numerical value for HfC
1	Lattice constant (nm)	0.456
2	Orientation of central facet	(001)
3	Nearest-neighbour separation in central facet (nm)	0.322
4	Separation of FIM image-spot centres on FIM screen (mm)	0.76
5	Deduced linear magnification of FIM	2.36×10^6
6	FEM image-spot radius on FEM screen (with beam broadening) (mm)	2.95
7	Estimated spot-radius correction factor	1/1.2
8	Estimated FEM image-spot radius on FEM screen (without beam broadening) (mm)	2.46
9	Estimated radius ρ^S of FE electron source on emitter (using FIM linear magnification) (nm)	1.041
10	Derived FE electron source area A^S on emitter (nm^2)	3.41

Making reliable theoretical estimates of these beam effects is difficult, so we use Fig. 2(f) in Fink's1988 paper [45] on point sources to make an empirical estimate of the (maximum) linear-magnification difference between electrons and ions. Fink's Fig. 2(f) is a FEM image of a 3-atom tungsten tip, with the corresponding FIM image superimposed in reverse contrast. Measurement on an electronically enlarged version of Fink's Fig. 2(f) suggests that the ratio of his FEM image radius to his FIM image radius is approximately 1.2. Some of this difference may be caused if the two imaging processes image slightly different areas on the tip, but this figure of 1.2 should provide a maximum estimate of the bean broadening correction factor as it applies in Fink's experiment. Lacking better information, we assume it applies to our experiments, and that the "FEM screen-image radius without broadening" is obtained by dividing the "initial FEM screen--

image radius" (derived above) by the correction factor 1.2. Numerical details are in Table 1.

This result is then converted to a linear distance ρ^S on the emitter tip, using the linear magnification m_{lin} derived from the FIM experiments. This distance ρ^S is the apparent FE source radius on the tip (i.e. ρ^S is the extracted experimental value of the parameter $R_{emission}$ used in the simulations). Finally, in line 10, ρ^S is converted to a corresponding electron-source area A^S, by ignoring small complications due to emitter-tip curvature and using $A^S=\pi\{\rho^S\}^2$. The final result is $A^S \sim 3.4$ nm^2.

We think it possible that details of the electron optics of the linkage between the channel plate and the microscope screen could mean that the image-spot radius at the microchannel-plate entry plane is not exactly equal to the image-spot radius on the microscope phosphor screen. This would require a more careful analysis and a further correction factor. However, any such factor is expected to be very close to unity, and should not affect the final conclusions below.

3.3 Emission area derived by FN-plot analysis

Using the method of Section 2.3, the formal emission area of the HfC emitter has been extracted from a FN plot, using the alternative assumptions of (a) an ET barrier and (b) a SN barrier. Fig. 3(a) shows the current-voltage data collected, and Fig. 3(b) the related FN plot.

Results are shown in Table 2. Lines 2 to 8 report experimental data as derived from the relevant FN plot.

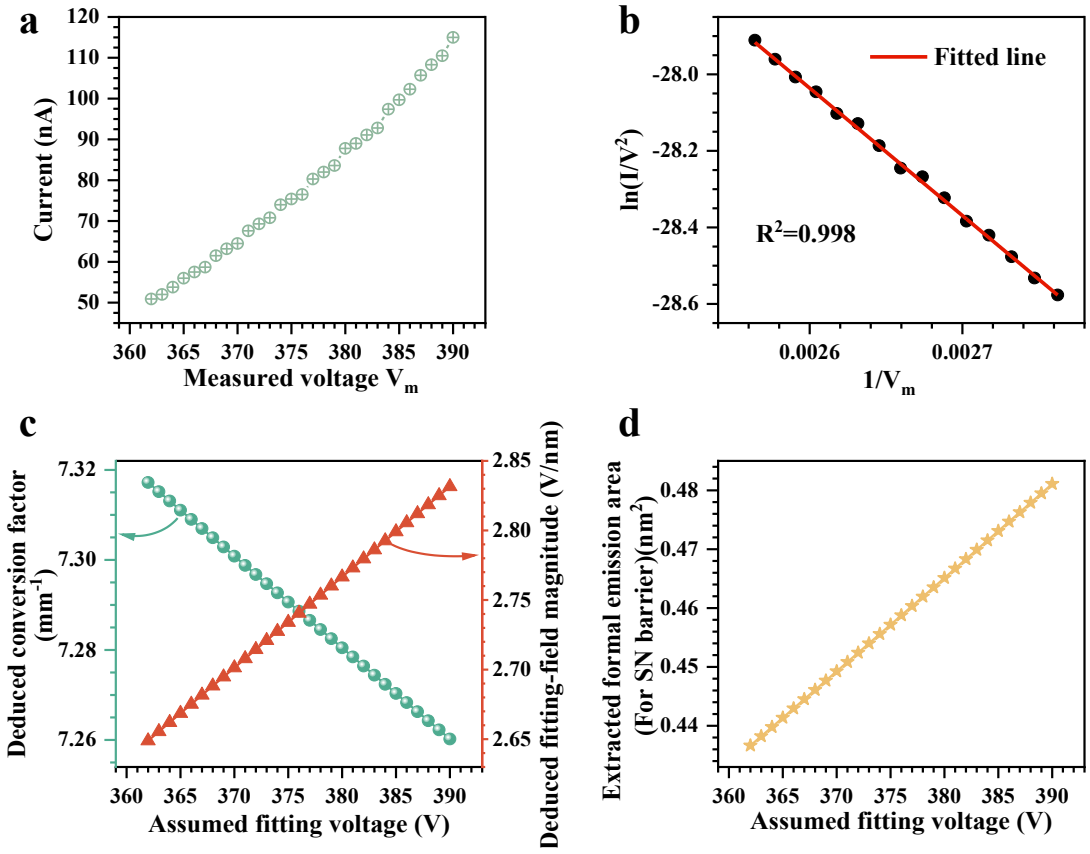


Fig. 3. (a) Current-voltage measurements for HfC emitter. (b) Related FN plot. (c) To show how the extracted values of conversion factor and fitting field depend on the value chosen for the fitting voltage. (d) To show how the extracted value of formal emission A_f^{SN} depends on the value chosen for the fitting voltage.

Results are shown in Table 2. Lines 2 to 8 report experimental data as derived from the relevant FN plot. As explained earlier, in the SN barrier case the extracted values of β and A_f^{SN} depend on what value is assumed for the "fitting value" V_t of measured voltage: for a given fitting voltage, an iteration procedure (described in Section 4.2 and the ESM) is used to establish the corresponding values of β, F_t, f_t, s_t and r_t. Line 9 in Table 2 reports the "starting value" β_1 used in these iterations.

Consequences of this need to decide V_t are illustrated in Figs 3(c) and 3(d). The effect on the extracted value of β is slight (the range is about 1%). However, due to the "lever effect" that occurs with semi-logarithmic plots, the effect on the extracted value of A_f^{SN} is more significant (the range is about 10%).

As a convenient "definitive" approximation, we take V_t to be the mid-range voltage V_{mid} recorded on line 7 of Table 2. Lines 10 to 15 report the corresponding values of β, F_t, f_t, s_t, r_t, and $r_t s_t^2$. Lines 16 and 17 show the corresponding extracted values of A_f^{ET} and A_f^{SN}.

The true fitting value of measured voltage will be slightly higher than V_{mid}, so using (instead) the voltage-range maximum will provide a maximum bound (here 6%) on the error associated with using the mid-range value. Details are provided on lines 18 and 19. This uncertainty is unavoidable when FN plots are used.

Table 2: Data relating to comparison of emission areas.		
Line	Parameter	Numerical value for HfC [25]
1	Assumed local work function ϕ (eV)	2.50
2	Vertical axis intercept $\ln\{R^{\mathrm{expt}}\}$	–19.38
3	R^{expt} (A/V^2)	3.832×10^{-9}
4	FN plot slope S^{expt} (Np V)	–3329
5	$R^{\mathrm{expt}}\cdot(S^{\mathrm{expt}})^2$ (A)	4.246×10^{-2}
6	Experimental voltage range (V)	362–390
7	Mid-range experimental voltage V^{mid} (V)	376
8	Related experimental current I (nA)	75
9	CF starting value β_{I} (nm^{-1})	1.000×10^{-3}
10	Extracted CF value β (nm^{-1}) [assuming V_{mid} as the fitting voltage]	7.26×10^{-3}
11	Fitting value F_{t} of apex field (V/nm)	2.73
12	Fitting value f_{t} of apex scaled field	0.629
13	Fitting value s_{t} of slope correction factor	0.892
14	Fitting value r_{t} of intercept correction factor	282
15	Value of $r_{\mathrm{t}}s_{\mathrm{t}}^2$	224
16	Formal emission area extracted using ET barrier $A_{\mathrm{f}}^{\mathrm{ET}}$ (nm^2)	90
17	"Mid-range" formal emission area extracted using SN barrier $A_{\mathrm{f}}^{\mathrm{SN}}$ (nm^2)	0.46
18	Highest limit for $A_{\mathrm{f}}^{\mathrm{SN}}$ (nm^2)	0.488
19	Upper bound on extraction error for $A_{\mathrm{f}}^{\mathrm{SN}}$	6 %
	Comparisons using present data	
20	$A_{\mathrm{f}}^{\mathrm{ET}}/A^{\mathrm{S}}$	~ 25
21	$A^{\mathrm{S}}/A_{\mathrm{f}}^{\mathrm{SN}}$	~ 7.4
	Corresponding Ehrlich & Plummer data [38]	
22	$j_{\mathrm{m}}/j_{\mathrm{EL}}$	~ 20–40
23	$j_{\mathrm{MG}}/j_{\mathrm{m}}$	~ 4.4–4.8

Lines 20 and 21 in Table 2 then use ratios to compare the emission area A^{S} extracted from the FIM and FEM experiments with the results obtained from FN plots as analysed using ET and SN barriers. Clearly, the FIM/FEM experimental result is much closer to the SN barrier theoretical result. These new results are qualitatively consistent with the older results of Ehrlich and Plummer, shown in Lines 22 and 23.

4. General discussion

4.1 Some implications of accepting MG theory

There are various implications when experimentalists use EMG FE theory (rather than elementary FE theory) to analyse their experimental current-voltage data.

4.1.1 Some implications for single-tip field emitters (STFEs)

As already indicated, extraction of voltage-to-local-field conversion factors (β-values) is only slightly affected by the use of EMG FE theory - extracted values are typically roughly around 5% higher when using elementary FE theory. However, using elementary theory leads to over-prediction of extracted formal area by a factor of order 100 or more and under-prediction of local emission current density and hence emission currents by a factor of 100 or more. Such errors could be highly unfortunate in research-and-development contexts – for example when trying to report the effectiveness of some new form of emitter, or to predict the occurrence of field-emission-initiated electrical breakdown. For professional engineers, use of theory known to be seriously incorrect might be considered irresponsible behaviour.

A context where MG FE theory has long been used is electron-optical theory. An important parameter [10] is the parameter d_F called here the "D-decay width at the Fermi level". This is defined and given (in MG FE theory) by

$$d_F \equiv 1/\left[(-\partial \ln D/\partial H)|_{H=\phi}\right] = t^{-1} \cdot (2/3b)(F/\phi^{1/2}) \ , \qquad (8)$$

where D is the tunnelling probability for a SN barrier of zero-field height H, b is the second FN constant as before, and t is the parameter that appears in the pre-exponential of the 1956 MG FE equation. The combination $(2/3b)$ is a universal constant with the value 9.760 $eV^{3/2}\,(V/nm)^{-1}$, and t can usually be approximated (to the nearest 5%) as 1.05. The parameter d_F plays an important role in the theoretical prediction of energy distributions [10], in particular the room-temperature total-energy distribution (TED) [46] shown in Fig. 4(a).

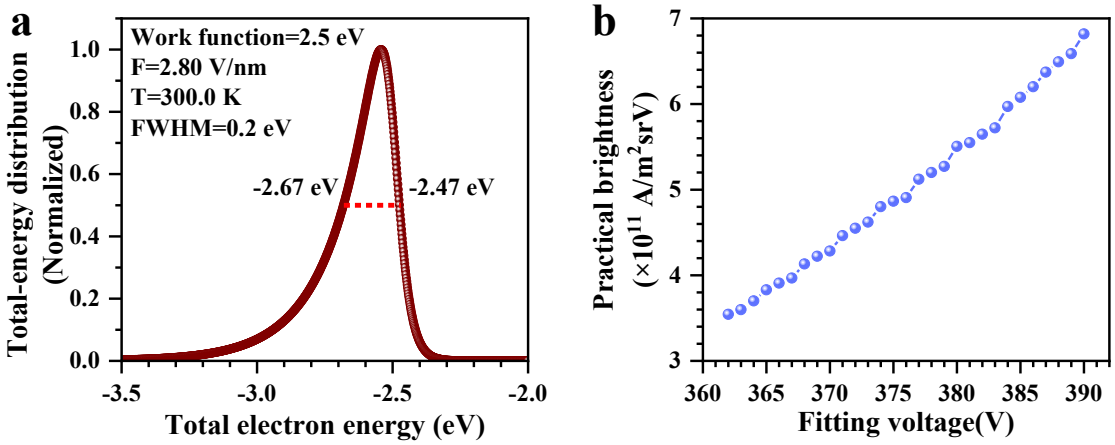


Fig. 4. (a) Predicted normalized room-temperature total-energy distribution (TED) for 2.5 eV work-function emitter, at surface field of 2.8 V/nm. (b) To show how the practical brightness B_{pract} extracted using eq. (11) depends on the value chosen for the fitting voltage V_{t}.

Another parameter of electron-optical interest is the "practical brightness" B_{pract} discussed in Ref. 11 and estimated in the present context by

$$B_{\mathrm{pract}} \approx 1.44\, J^{\mathrm{extr}}/\pi d_{\mathrm{F}} \approx (1.44/\pi d_{\mathrm{F}})(I_{\mathrm{m}}/A_{\mathrm{f}}^{\mathrm{SN}}) \ , \tag{9}$$

where J^{extr} $[\equiv I_{\mathrm{m}}/A_{\mathrm{f}}^{\mathrm{SN}}]$ is the "extracted LECD". Because both $A_{\mathrm{f}}^{\mathrm{SN}}$ and this extracted LECD value depend on the value assumed for the fitting voltage V_{t}, the value of B_{pract} derived from eq. (9) will also depend on the value assumed for V_{t}, as shown in Fig. 4(b).

4.1.2 Extraction of formal area efficiency

For FN plots, the extraction arguments above also apply to so-called large area field electron emitters (LAFEs), which contain very large numbers of individual emission sites.

For LAFEs, an additional parameter, namely the extracted *formal area efficiency* $\alpha_{\mathrm{f}}^{\mathrm{SN}}$ can be defined by

$$\alpha_{\mathrm{f}}^{\mathrm{SN}} \equiv A_{\mathrm{f}}^{\mathrm{SN}}/A_{\mathrm{M}} \ , \tag{10}$$

where A_{M} is the LAFE *macroscopic area* (or "footprint"). This parameter $\alpha_{\mathrm{f}}^{\mathrm{SN}}$ is a measure of what proportion of the emitter surface is actually emitting electrons. It is not an accurate measure, but looks a useful parameter when making comparisons in emitter research and development.

Formal area efficiencies have been calculated from measurements on several typical FE film cathodes. Results summarized in Table 3 suggest that emitter performance could probably be improved if fabrication procedures could be optimized.

Table 3: Formal emission area and formal area efficiency (derived by assuming a SN barrier), for several film-type large-area field electron emitters.			
Material and reference	CNT [47]	ZnO [21]	Mo [48]
Work function (eV)	4.6	3.3	4.7
Substrate area A_{M} (mm^2)	0.92	500	6.25
Extracted formal emission area $A_{\mathrm{f}}^{\mathrm{SN}}$ (nm^2)	8×10^{6}	2.3×10^{4}	5.5×10^{3}
Extracted formal area efficiency $\alpha_{\mathrm{f}}^{\mathrm{SN}}$	8.70×10^{-6}	4.6×10^{-11}	8.8×10^{-10}

4.2 Availability of computer program

To get good results for the extracted formal emission area $A_{\mathrm{f}}^{\mathrm{SN}}$, an iteration process is needed. For an assumed value of fitting voltage V_{t}, this iteration finds a self-consistent value for the voltage-to-local-field conversion factor β. The iteration loop is illustrated in Fig. 5. The parameter s_{t} is the fitting value of the slope correction factor, "i" is the iteration label, and F and G are functions defined in the ESM.

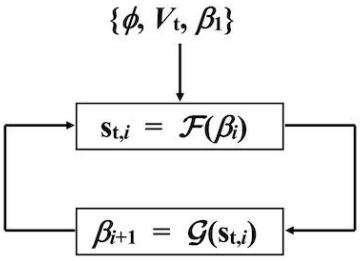


Fig. 5. To show structure of the iteration loop used for finding precise estimates of the parameters f_{t} and s_{t}, and of the conversion factor β, for a given value of fitting voltage V_{t}.

A program has been built that takes the necessary input data including the parameters S^{expt} and R^{expt}, and carries out this iteration. For selected values of V_{t} it generates corresponding estimates of f_{t}, s_{t}, β, F_{t}, r_{t}, $A_{\mathrm{f}}^{\mathrm{SN}}$, d_{F} and B_{pract}. A second part of the program employs user-inputs of local work function, temperature and field, and equations given by Swanson and Schwind [10], to calculate the related total-energy distribution, as shown in Fig. 4(a).

More information about the program is provided in the ESM. This program is freely available. The related .exe file and "users' manual" can be downloaded from https://www.tangshuai-fe-sysu.org.cn/survey.html. We hope that the availability of this easy-to-use program will encourage experimental FE researchers to use EMG FE theory, rather than elementary FE theory, to analyse FE experimental current-voltage data plotted as a FN plot.

4.3 Strength of FIM-FEM method and limitations of MG FE theory

Finally, we note that EMG FE theory is a planar FE theory that also disregards the role of atomic-level wave-functions. It will eventually be necessary to go beyond MG FE theory, as partially demonstrated by the work [49, 50] of Kyritsakis and colleagues on FE from Earthed spherical emitters. If practical emitters become ultrasharp or atomic-scale, then existing plot-based data-analysis methods will not work. However, the FIM-FEM method can be used to obtain the electron source area even at the near-atomic scale. Thus, this method is expected to be useful for characterizing upcoming atomic-scale sharply pointed electron sources.

5. Conclusions

This paper has introduced a new FIM-FEM experimental method for finding the electron source area A^{S} of an operating field electron emitter. It finds that A^{S} is much closer to the formal emission area $A_{\mathrm{f}}^{\mathrm{SN}}$ derived in FN-plot analysis by assuming a SN tunnelling barrier than to the formal emission area $A_{\mathrm{f}}^{\mathrm{ET}}$ derived by assuming an ET barrier. This seems welcome additional experimental confirmation that MG FE theory (based on the SN barrier) is better physics than elementary FE theory or 1920s FE theory, both based on the ET barrier, and that $A_{\mathrm{f}}^{\mathrm{SN}}$ is the better estimate of emission area.

The "messy" procedure needed when using MG FE theory to analyse FN plots has been packaged into a simple program that implements an iterative method. For various assumed fitting values of measured voltage, this program can extract/calculate important characteristics of FE sources, including apex field strength, apex FEF, formal emission area, the total-energy distribution (and hence its full width at half-maximum), and source practical brightness.

The program also determines the formal area efficiency of a large-area field electron emitter: this provides a measure of the efficiency of a film cathode. We hope that the availability of an easy-to-use program will encourage experimental FE researchers to use EMG FE theory, rather than elementary FE theory, to analyse FE experimental current-voltage data plotted as a FN plot. Finally, as already noted, because our new FIM-FEM method will work for apex-radius values smaller than those at which FN-plot-based methods become invalid, we expect our new method to be useful for characterizing upcoming atomic-scale sharply pointed electron sources.

6. Acknowledgement

This work was supported by the National Key Basic Research Program of China (Grant no. 2024YFA1209004), the National Natural Science Foundation of China (Grant no. 62301619, 62274188), the Key field Research Program of Guangdong Province (Grant no.

2022B0303030001), the Special Topic on Basic and Applied Basic Research of Guangzhou (Grant no. Grant no. 2024A04J4525), the Guangdong Provincial Association for Science and Technology Young Scientific and Technological Talent Cultivation Program, the Fundamental Research Funds for the Central Universities, Sun Yat-sen University (Grant no. 24hytd002-2) and start-up funds for the Central Universities, Sun Yat-sen University.

Supplementary Materials

We provide as Electronic Supplementary Material a detailed account of the present state of that part of field electron emission theory that is directly relevant to the main paper, as well as the evaluation of the fitting parameters of computer program.

Contributions

S.Z. Deng, N.S. Xu and S. Tang conceived and designed the study. S. Tang designed and performed the FIM-FEM experiments and electron-optic simulations. S. Tang and M.K. Gou write the program. M.K. Gou and Y.Z. Hu helped with electron-optic simulations. J. Tang and L.-C. Qin helped with FIM-FEM experiments. Y. Zhang and Y. Shen helped with results discussion. R.G. Forbes provided theoretical guidance about MG and FN theory. S. Tang, M.K. Gou, Y.Z. Hu, N.S. Xu, R.G. Forbes, S.Z. Deng analysed the data. S. Tang write the original paper and R.G. Forbes and S.Z. Deng revised the paper with input from all authors.

Declaration of competing interest

The authors declare that they have no known competing financial interests or personal relationships that could have appeared to influence the work reported in this paper.

Data availability

The data that support the findings of this study are available from the corresponding authors upon reasonable request.

References

1. Samavedam, S.B., Ryckaert, J., Beyne, E., Ronse, K., Horiguchi, N., Tokei, Z., Radu, I., Bardon, M.G., Na, M.H., Spessot, A. & Biesemans, S., Future logic scaling: towards atomic channels and deconstructed chips. *IEEE International Electron Devices Meeting*, 1.1.1–1.1.10 (2020).
2. Jeong, J., Lee, S.H., Masuoka, S.A., Min, S., Lee, S., Kim, S., Myung, T., Choi, B., Sohn, C.W., Kim, S.W., Choi, J., Park, J., Lee, H., Kim, T., Kim, S., Yasuda-Masuoka, Y., Ku, J.H. & Jeong, G., World's first GAA 3 nm foundry platform technology (Sf3) with novel multi-bridge-channel-FET (Mbcfet™) process. *IEEE Symposium on VLSI Technology and Circuits*, 1–2 (2023).

3. Nakane, T., Kotecha, A., Sente, A., Mcmullan, G., Masiulis, S., Brown, P.M.G.E., Grigoras, I.T., Malinauskaite, L., Malinauskas, T., Miehling, J., Uchański, T., Yu, L., Karia, D., Pechnikova, E.V., De Jong, E., Keizer, J., Bischoff, M., Mccormack, J., Tiemeijer, P., Hardwick, S.W., Chirgadze, D.Y., Murshudov, G., Aricescu, A.R. & Scheres, S.H.W., Single-particle Cryo-EM at atomic resolution. *Nature* **587**, 152–156 (2020).
4. Luque, D. & Castón, J.R., Cryo-electron microscopy for the study of virus assembly. *Nat. Chem. Biol.* **16**, 231–239 (2020).
5. Danz, T., Domröse, T. & Ropers, C., Ultrafast nanoimaging of the order parameter in a structural phase transition. *Science* **371**, 371–374 (2021).
6. Yang, J., Zeng, Z., Kang, J., Betzler, S., Czarnik, C., Zhang, X., Ophus, C., Yu, C., Bustillo, K., Pan, M., Qiu, J., Wang, L.-W. & Zheng, H., Formation of two-dimensional transition metal oxide nanosheets with nanoparticles as intermediates. *Nat. Mater.* **18**, 970–976 (2019).
7. Sawada, H., Tanishiro, Y., Ohashi, N., Tomita, T., Hosokawa, F., Kaneyama, T., Kondo, Y. & Takayanagi, K., STEM imaging of 47-pm-separated atomic columns by a spherical aberration-corrected electron microscope with a 300-kV cold field emission gun. *Microscopy* **58**, 357–361 (2009).
8. Morishita, S., Ishikawa, R., Kohno, Y., Sawada, H., Shibata, N. & Ikuhara, Y., Resolution achievement of 40.5 pm in scanning transmission electron microscopy using 300 kV microscope with delta corrector. *Microsc. Microanal.* **24**, 120–121 (2018).
9. Nabben, D., Kuttruff, J., Stolz, L., Ryabov, A. & Baum, P., Attosecond electron microscopy of sub-cycle optical dynamics. *Nature* **619**, 63–67 (2023).
10. Swanson, L.W. & Schwind, G., A review of the cold-field electron cathode. *Adv. Imaging Electron Phys.* **159**, 63–100 (2009).
11. Bronsgeest, M., Barth, J., Swanson, L. & Kruit, P., Probe current, probe size, and the practical brightness for probe forming systems. *J. Vac. Sci. Technol. B* **26**, 949–955 (2008).
12. Bacovský, J., Aberration correction for low voltage optimized transmission electron microscopy. *MethodsX* **5**, 1033–1047 (2018).
13. Haider, M., Uhlemann, S., Schwan, E., Rose, H., Kabius, B. & Urban, K., Towards 0.1 nm resolution with the first spherically corrected transmission electron microscope. *Nature* **392**, 768–769 (1998).
14. Batson, P., Dellby, N. & Krivanek, O., Sub-ångström resolution using aberration corrected electron optics. *Nature* **418**, 617–620 (2002).
15. Smith, D.J., Ultimate resolution in the electron microscope? *Mater. Today* **11**, 30–38 (2008).
16. Fowler, R.H. & Nordheim, L., Electron emission in intense electric fields. *Proc. R. Soc. Lond. A* **119**, 173–181 (1928).
17. Swanson, L.W., Current fluctuations from various crystal faces of a clean tungsten field emitter. *Surf. Sci.* **70**, 165–180 (1978) .
18. Swanson, L.W. & Crouser, L.C., Anomalous total-energy distribution for a molybdenum field emitter. *Phys. Rev. Lett.* **19**, 1179–1181 (1967).
19. Hsieh, C.-T., Chen, J.-M., Lin, H.-H. & Shih, H.-C., Field emission from various CuO nanostructures. *Appl. Phys. Lett.* **83**, 3383–3385 (2003).
20. Zhou, J., Xu, N.S., Deng, S.Z., Chen, J., She, J.C. & Wang, Z.L., Large-area nanowire arrays of molybdenum and molybdenum oxides: synthesis and field emission properties. *Adv. Mater.* **15**, 1835–1840 (2003).
21 Wang, L.B., Zhao, Y.Y., Zheng, K.S., She, J.C., Deng, S.Z., Xu, N.S. & Chen, J., Fabrication of large-area ZnO nanowire field emitter arrays by thermal oxidation for high-current application. *Appl. Surf. Sci.* **484**, 966–974 (2019).

22. De Jonge, N., Lamy, Y., Schoots, K. & Oosterkamp, T.H., High brightness electron beam from a multi-walled carbon nanotube. *Nature* **420**, 393–395 (2002).
23. Tang, S., Zhang, Y., Zhao, P., Zhan, R.Z., Chen, J. & Deng, S.Z., Realizing the large current field emission characteristics of single vertical few-layer graphene by constructing a lateral graphite heat dissipation interface. *Nanoscale* **13**, 5234–5242 (2021).
24. Mamishin, S., Kubo, Y., Cours, R., Monthioux, M. & Houdellier, F., 200 keV cold field emission source using carbon cone nanotip: application to scanning transmission electron microscopy. *Ultramicroscopy* **182**, 303–307 (2017).
25. Tang, S., Tang, J., Chiu, T.-W., Hayami, W., Uzuhashi, J., Ohkubo, T., Uesugi, F., Takeguchi, M., Mitome, M. & Qin, L.-C., A HfC nanowire point electron source with oxycarbide surface of lower work function for high-brightness and stable field-emission. *Nano Res.* **13**, 1620–1626 (2020).
26. Chiu, T.-W., Tang, J., Tang, S., Yuan, J. & Qin, L.-C., Synthesis and field emission of ZrC nanowire. *Mater. Today Commun.* **25**, 101240 (2020).
27. Kagarice, K.J., Magera, G.G., Pollard, S.D. & Mackie, W.A., Cold field emission from HfC(310). *J. Vac. Sci. Technol. B* **26**, 868–871 (2008).
28. Tang, S., Tang, J., Uzuhashi, J., Ohkubo, T., Hayami, W., Yuan, J., Takeguchi, M., Mitome, M. & Qin, L.-C., A stable LaB_6 nanoneedle field-emission point electron source. *Nanoscale Adv.* **3**, 2787–2792 (2021).
29. Tang, S., Tang, J., Wu, Y., Chen, Y.-H., Uzuhashi, J., Ohkubo, T. & Qin, L.-C., Stable field-emission from a CeB_6 nanoneedle point electron source. *Nanoscale* **13**, 17156–17161 (2021).
30. Gou, M.K., Tang, S., Huang, K., Guan, H.K., Zhan, R.Z., Liang, C.L., Chen, C.C., Shen, Y. & Deng, S.Z. Ultrabright LaB_6 nanoneedle field emission electron source with low vacuum compatibility. *Commun. Mater.* **6**, 133 (2025).
31. Zhang, H., Tang, J., Yuan, J., Yamauchi, Y., Suzuki, T.T., Shinya, N., Nakajima, K. & Qin, L.-C., An ultrabright and monochromatic electron point source made of a LaB_6 nanowire. *Nat. Nanotechnol.* **11**, 273–279 (2016).
32. Tang, S., Tang, J., Okunishi, E., Ninota, Y., Yasuhara, A., Uzuhashi, J., Ohkubo, T., Takeguchi, M., Yuan, J., & Qin, L.-C., A stable LaB_6 nanoneedle field-emission electron source for atomic resolution imaging with a transmission electron microscope. *Mater. Today* **57**, 35–42 (2022).
33. Nordheim, L.W. The effect of the image force on the emission and reflexion of electrons by metals. *Proc. R. Soc. Lond.* **A121**, 626–639 (1928).
34. Forbes, R.G. Comments on the continuing widespread and unnecessary use of a defective emission equation in field emission related literature. *J. App. Phys.* **126,** 210901 (2019).
35. Burgess, R.E, Kroemer, H. & Houston, J.M. Corrected values of Fowler-Nordheim field emission functions $\nu(y)$ and $s(y)$. *Phys. Rev.* **90**, 515 (1953).
36. Murphy, E.L & Good, R.H. Thermionic emission, field emission, and the transition region. *Phys. Rev.*, **102,**14641473 (1956).
37. Forbes, R.G. Renewing the mainstream theory of field and thermal electron emission. Chapter 9 (pp. 387–447) in: G. Gaertner, W. Knapp and R.G. Forbes (eds) *Modern Developments in Vacuum Electron Sources* (Springer Nature, Switzerland, 2020).
38. Ehrlich, C.D. & Plummer, E.W., Measurement of the absolute tunneling current density in field emission from tungsten (110). *Phys. Rev. B* **18**, 3767–3771 (1978).
39. Forbes. R.G. & Deane, J.H.B. Comparison of approximations for the principal Schottky-Nordheim barrier function $\nu(f)$, and comments on Fowler-Nordheim plots. *J. Vac. Sci. Technol. B* **28**, C2A33–42 (2010).
40. Forbes, R.G. The Murphy-Good plot: a better method of analysing field emission data. *R. Soc. Open Sci.* **6**,

190912 (2019).
41. Forbes, R.G. Development of a simple quantitative test for lack of field emission orthodoxy, *Proc. R. Soc. Lond. A* **469**, 20130271 (2013).
42. Forbes. R.G. & Deane, J.H.B. Refinement of the extraction-parameter approach for deriving formal emission area from a Fowler-Nordheim plot. *30th International Vacuum Nanoelectronics Conf.*, Regensburg, July 2017.
43. Nicholas, F. *Atlas of Models of Crystal Surfaces* (Taylor and Francis, London, 1965).
44. Hawkes, P.W. & Kasper, E. Principles of Electron Optics, Vol 2: Applied Geometrical Optics (Academic, London, 1996).
45. Fink, H.W. Point source for ions and electrons. *Phys. Scr.* **38**, 260–263 (1988).
46. Young, R.D. Theoretical total-energy distribution of field-emitted electrons. *Phys. Rev.* **113**, 110–114 (1959).
47. Calderón-Colón, X., Geng, H., Gao, B., An, L., Cao, G., & Zhou, O. A Carbon Nanotube Field Emission Cathode with High Current Density and Long-Term Stability. *Nanotechnology* **20**, 325707 (2009).
48. Whaley, D.R., Duggal, R., Armstrong, C.M., Bellew, C.L., Holland, C.E. & Spindt, C.A.100 W Operation of a Cold Cathode TWT. *IEEE Trans. Electro. Dev.* **56**, 896-905 (2009).
49. Kyritsakis, A. & Xanthakis, J.P. Derivation of a generalized Fowler-Nordheim equation for nanoscopic field-emitters, *Proc. R. Soc. Lond. A* **471**, 20140811 (2015).
50. Kyritsakis, A. & Djurabekova, F. A general computational method for electron emission and thermal effects in field emission nanotips. *Computational Mater. Sci.* **128**, 15–21 (2017).

Supplementary Files

This is a list of supplementary files associated with this preprint. Click to download.

- SupplementaryMaterialsMethodsforcharacterizationofatomicscalefieldemissionpointelectronsource.docx